# Study of the EEC discrimination power on quark and gluon jet quenching effects in heavy-ion collisions at $\sqrt{s}$ = 5.02 TeV*

Shi-Yong Chen (陈时勇)[1,2] Zi-Xuan Xu (徐子璇)[2] Ke-Ming Shen (申可明)[3] Wei Dai (代巍)[4†]
Ben-Wei Zhang (张本威)[2] Enke Wang (王恩科)[5,2]

[1]Huanggang Normal University, Huanggang 438000, China
[2]Key Laboratory of Quark & Lepton Physics (MOE) and Institute of Particle Physics, Central China Normal University, Wuhan 430079, China
[3]East China University of Technology, Nanchang 330013, China
[4]School of Mathematics and Physics, China University of Geosciences, Wuhan 430074, China
[5]Guangdong Provincial Key Laboratory of Nuclear Science, Institute of Quantum Matter, South China Normal University, Guangzhou 510006, China

**Abstract:** We present a systematic investigation of flavor-dependent jet quenching using energy-energy correlators (EEC) in $\sqrt{s}$ = 5.02 TeV Pb+Pb collisions. Employing the improved SHELL model, which incorporates collisional and radiative energy loss, as well as medium response, we quantify distinct quenching signatures for quark and gluon jets. Key findings include: (1) Pure quark jets exhibit strong EEC enhancement at large angular scales, while gluon jets show a bimodal enhancement pattern at small and large scales; (2) Dual-shift decomposition in the EEC ratio reveals shifts toward large angles is primarily driven by energy loss, while small-$R_{\rm L}$ shifts extend beyond selection bias and indicate intrinsic enhancement of the gluon-initiated jets; (3) Quark jets experience global suppression of averaged energy weight $\langle \text{weight} \rangle(R_{\rm L})$, whereas gluon jets exhibit concentration toward small $R_{\rm L}$; (4) Mechanism decomposition identifies elastic energy loss concentrating $\langle \text{weight} \rangle(R_{\rm L})$ toward small $R_{\rm L}$, radiative loss dominating quark jet modification, and medium response amplifying large $R_{\rm L}$ enhancement via soft hadrons. The observed flavor dependence in EEC modifications is dominantly driven by intrinsic jet structure differences rather than medium-induced mechanisms. We propose photon-tagged jets as quark proxies and inclusive charged-hadron jets as gluon proxies, demonstrating that they reproduce the respective flavor-specific quenching patterns. Our work establishes the EEC as a precision probe of color-charge-dependent jet-medium interactions, providing new constraints for the detailed $\hat{q}$ extraction and QGP tomography, while highlighting the critical role of pre-quenching flavor asymmetries.

**Keywords:** jet quenching, heavy ion, jet substructure

**DOI:** 10.1088/1674-1137/ae056c **CSTR:** 32044.14.ChinesePhysicsC.50023114

## I. INTRODUCTION

The creation of a deconfined quark-gluon plasma (QGP) in relativistic heavy-ion collisions provides a unique opportunity to study quantum chromodynamics (QCD) under extreme conditions in a laboratory [1–5]. Highly energetic jet-collimated sprays of particles, resulting from the fragmentation of hard-scattered partons produced in the initial collisions, serve as precision probes to the novel properties of this QCD medium. The phenomenon of jet quenching, characterized by the significant suppression of high-transverse momentum ($p_{\rm T}$) hadrons and jets relative to scaled proton-proton collisions, arises primarily from parton energy loss mechanisms such as medium-induced gluon radiation and elastic collisions [6–8]. Quantifying this energy loss provides critical, direct insights into the QGP's transport coefficients. To dissect the complex space-time evolution of the in-medium parton shower and differentiate between competing energy loss mechanisms, jet substructure observables have emerged as indispensable, high-resolution tools [9–35]. These observables quantify the modification of the jet's internal energy flow and fragmentation pattern caused by interactions with the QGP. Recent significant advances include detailed measurements of differential jet shapes [26, 27, 36–38], fragmentation functions

Received 19 June 2025; Accepted 4 September 2025; Accepted manuscript online 5 September 2025

* This research is supported by the Guangdong Major Project of Basic and Applied Basic Research (2020B0301030008) and the National Natural Science Foundation of China with Project (11935007, 12035007). Ke-Ming Shen is supported by the Doctoral Research of ECUT ( DHBK2019211)

† E-mail: weidai@mail.cug.edu.cn

[39–42], and groomed jet observables [21, 43], which collectively offer a multi-dimensional tomography of jet-medium interactions.

Among jet substructure observables, the energy-energy correlator (EEC) [44–47] is particularly significant due to its sensitivity to soft and collinear radiation patterns within jets. Defined as the energy-weighted angular correlation between particle pairs, the EEC probes jet internal structure in elementary collisions and has emerged as a powerful tool for studying QCD dynamics [48–74]. In heavy-ion collisions, it elucidates the onset of color coherence in medium-induced splittings [75–82], reveals the medium response effect, mass hierarchy in heavy-flavor jets [83–86], and exposes cold nuclear matter effects in small systems [87–89]. The impact of selection bias on the modification of the EEC is also discussed in [90, 91]. Moreover, EEC has also garnered significant attention among experimentalists [92–95], with STAR, CMS, and ALICE collaborations conducting dedicated measurements of this observable in heavy-ion collisions.

Flavor-dependent parton energy loss is a fundamental aspect governing jet evolution within the QGP [7, 96]. Distinct Casimir color factors not only lead to differences in the magnitude of energy loss between quarks and gluons but also subject them to differential in-medium splitting [97–100]. This inherent difference in energy loss rates manifests directly as distinct medium modifications in jet substructure observables such as jet charge [29, 101, 102] and jet shape [32, 36, 37, 103]. However, a detailed understanding of how quark-gluon differences manifest in the in-medium radiation pattern of jet substructure observables in heavy-ion collisions is absent. Therefore, it is compelling to investigate the flavor-dependent jet quenching patterns within finer in-jet substructure using the EEC.

The remainder of the paper is organized as follows. In Sec. II, we introduce the definition of the EEC used for the ALICE experimental study, and the p+p baseline of the EEC distributions for inclusive jets in three different jet transverse momentum intervals is calculated to compare with the experimental data. In Sec. III we calculate and compare the EEC distributions for inclusive jets in Pb+Pb and p+p at $\sqrt{s} = 5.02$ TeV for the transverse momentum interval $40-60$ GeV, to derive medium modification ratios (A+A/p+p). The in-depth phenomenology exploration of such an observable is also presented and aids in discussing differences in the jet quenching of quark- and gluon-initiated jets from the following four aspects: their respective EEC distributions, the effect of different jet quenching mechanisms on them, the different modifications of the fine structures revealed by the intra-jet EEC, and their different selection bias effects. Finally, we present the summary in Sec. IV.

## II. EEC DISTRIBUTIONS IN P+P COLLISIONS

The ALICE defined EEC describes the energy-weighted cross-section of particle pairs as functions of the angular distance between each pair as follows [95]:

$$\Sigma_{\rm EEC}(R_{\rm L}) = \frac{1}{N_{\rm jet}\cdot\Delta R}\int_{R_{\rm L}-\frac{1}{2}\Delta R}^{R_{\rm L}+\frac{1}{2}\Delta R}\sum_{\rm jets}\sum_{i,j}\frac{p_{{\rm T},i}p_{{\rm T},j}}{p^2_{\rm T,jet}}\delta(R'_{\rm L}-R_{{\rm L},ij})\,{\rm d}R'_{\rm L}\,, \tag{1}$$

where all final state particle pairs $(i, j)$ inside each jet are summed up. The angular distance between each pair is defined in the $\eta-\varphi$ plane as $R_{{\rm L},ij} = \sqrt{(\varphi_j-\varphi_i)^2+(\eta_j-\eta_i)^2}$, where $\Delta R$ is the angular bin width and $N_{\rm jet}$ is the total number of jets. It corresponds to a distribution observable defined in a jet.

We begin by calculating the defined EEC distributions of inclusive jets in p+p collisions to provide a baseline for further studies. In the work, we use a Monte Carlo (MC) event generator PYTHIA v8.309 [104] with Monash 2013 tune [105] to simulate jet productions in p+p collisions. To compare our calculated results with experimental data, we use the same kinematic cuts of events as adopted by the ALICE measurements [94]. All jets are reconstructed by the anti-$k_{\rm T}$ algorithm with radius parameter $R = 0.4$ from charged particles with $p_{\rm T} \geq 1$ GeV using the FASTJET v3.4.0 package [106]. The reconstructed jets are accepted in the transverse momentum range $20\ {\rm GeV} < p_{\rm T,jet} < 80$ GeV and rapidity range of $|\eta_{\rm jet}| < 0.5$. Our numerical results of $\Sigma_{\rm EEC}$ as functions of $R_{\rm L}$ for inclusive charged jets and their comparisons with ALICE data in p+p collisions at $\sqrt{s} = 5.02$ TeV are shown in Fig. 1.

We can observe that the Pythia simulation results show fairly good agreement with experimental measurements in p+p collisions in the three $p_{\rm T}$ intervals, which will serve as input and baseline for the subsequent study in Pb+Pb collisions. It is worth mentioning that the models incorporating high-order corrections can provide an improved description of the experimental data shown in [94]. The EEC distributions are shifted to a lower $R_{\rm L}$ region with the increasing jet $p_{\rm T}$. We can conclude that, with the increment of jet $p_{\rm T}$, the EEC distributions shift to smaller $R_{\rm L}$, and the height of the distribution will increase, which is affected by the different number of particle pairs within one jet in each $p_{\rm T}$ interval. To ex-

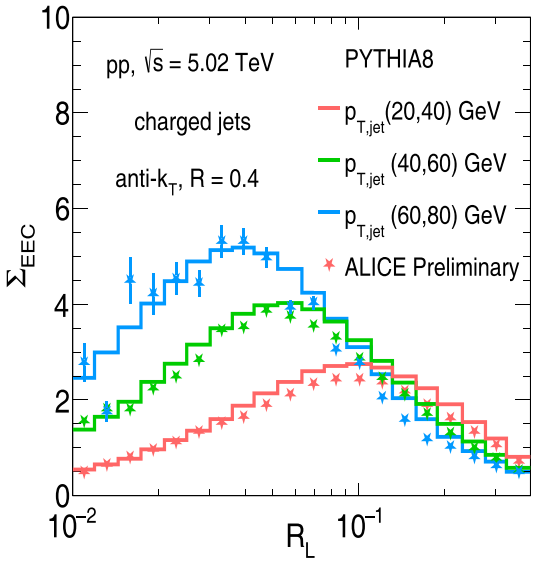


**Fig. 1.** (color online) PYTHIA8 simulation results of defined $\Sigma_{\rm EEC}$ distributions as functions of $R_{\rm L}$ for inclusive charged jets with a jet size of $R = 0.4$ in three jet transverse momentum intervals: $20\ {\rm GeV} < p_{\rm T,jet} < 40$ GeV, $40\ {\rm GeV} < p_{\rm T,jet} < 60$ GeV and $60\ {\rm GeV} < p_{\rm T,jet} < 80$ GeV produced in p+p collisions at $\sqrt{s} = 5.02$ TeV. The results are compared with the ALICE experimental data [94].

tract such an effect, it is natural to divide the EEC observable into two major parts, rewritten as

$$\Sigma_{\rm EEC}(R_{\rm L}) = \frac{N^{\rm total}_{\rm pair}}{N_{\rm jet}} \cdot \frac{\Delta N_{\rm pair}}{N^{\rm total}_{\rm pair}\Delta R}(R_{\rm L}) \cdot \langle {\rm weight} \rangle (R_L), \qquad (2)$$

where we average the energy weight term, $p_{{\rm T},i}p_{{\rm T},j}/p^2_{\rm T,jet}$, to each particle pair within each jet in each angular bin $\Delta R$, denoted as $\langle {\rm weight} \rangle$; therefore, we can simply replace the integration and then sum over jets and $i, j$ into a summed number of pairs within each bin $\Delta R$, denoted as $\Delta N_{\rm pair}$. Consequently, Eq. (2) appears as the averaged number of particles within a jet, normalized $R_{\rm L}$ distribution on the number of pairs, and the averaged energy weight distribution as a function of $R_{\rm L}$. This benefits further explorations and discussions.

We plot the $R_{\rm L}$ distributions of the total number of pairs normalized to every inclusive charged jet produced in p+p collisions at $\sqrt{s} = 5.02$ TeV for all three $p_{\rm T,jet}$ intervals in the upper panel of Fig. 2, denoted as the product of the first two terms in Eq. (2). The corresponding $R_{\rm L}$ distributions of the averaged weight $\langle {\rm weight} \rangle$ are also shown in the bottom panel of Fig. 2.

We find in the upper panel that most of the particle-pairs are distributed around $R_{\rm L} = 0.2$, and there is no jet transverse momentum dependence of the peak position. The distribution height increases with the enhancement of $p_{\rm T,jet}$ because the number of constituents within the jets

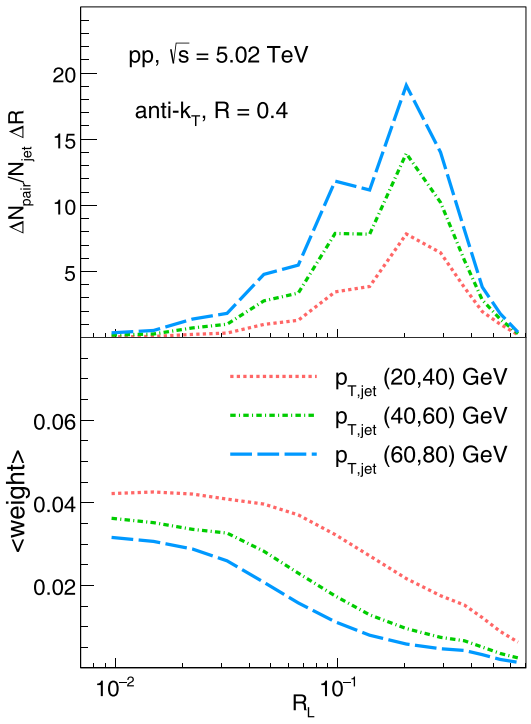


**Fig. 2.** (color online) Number of jets normalized pair-number distributions (upper panel) and averaged energy weight (lower panel) distributions as functions of $R_{\rm L}$ for inclusive charged jets in three jet transverse momentum intervals: $20\ {\rm GeV} < p_{\rm T,jet} < 40$ GeV, $40\ {\rm GeV} < p_{\rm T,jet} < 60$ GeV and $60\ {\rm GeV} < p_{\rm T,jet} < 80$ GeV produced in p+p collisions at $\sqrt{s} = 5.02$ TeV.

increases as a consequence. In the bottom panel, the role of the $\langle {\rm weight} \rangle$ is to shift the distribution of particle pairs toward smaller $R_{\rm L}$ directions while the heights of the $\langle {\rm weight} \rangle$ distribution are also determined by the jet transverse momentum. Higher jet transverse momentum leads to more constituent particles within the jet, consequently resulting in lower $\langle {\rm weight} \rangle$ values.

## III. EEC DISTRIBUTIONS IN A+A COLLISIONS

### A. Improved SHELL model

In relativistic heavy-ion collisions, partons produced from initial hard scatterings undergo energy loss through interactions with the QGP. To simulate this process, we employ the improved SHELL model —a Monte Carlo framework that concurrently handles both elastic and inelastic scattering processes and the medium response during jet propagation. The SHELL model has been quantitatively validated relative to multiple experimental observables, thereby establishing its reliability for jet quenching studies [32, 107–111]. The model initializes parton positions via sampling from a Glauber-model-based nuclear geometry [112], and subsequently they transport through the QGP step-by-step. The radiative energy loss mechan-

ism is implemented via a stochastic implementation approach. The probability of a gluon radiation when traversing through the QGP medium during each time step $\Delta t$ is expressed as

$$P_{\rm rad}(t,\Delta t) = 1 - {\rm e}^{-\langle N(t,\Delta t)\rangle}. \tag{3}$$

Here, $\langle N(t,\Delta t)\rangle$ is the averaged number of radiated gluons, which is calculated from the medium induced radiated gluon spectrum within the Higher-Twist (HT) method [113–116]:

$$\frac{{\rm d}N}{{\rm d}x\,{\rm d}k_\perp^2\,{\rm d}t} = \frac{2\alpha_s C_s P(x)\hat{q}}{\pi k_\perp^4}\sin^2\left(\frac{t-t_i}{2\tau_f}\right)\left(\frac{k_\perp^2}{k_\perp^2+x^2M^2}\right)^4, \tag{4}$$

where $\alpha_s$ is the strong coupling constant, $x$ and $k_\perp$ devote the energy fraction and the $p_{\rm T}$ of the radiated gluon, $M$ is the mass of the parent parton. Only the gluon with a lower $x_{\rm min} = \mu_D/E$ cut-off is allowed to emit, and $\mu_D$ is the Debye screening mass. $P(x)$ is the QCD splitting function in vacuum, $C_s$ denotes the Casimir factor for gluon ($C_A$) and quark ($C_F$). $\tau_f = 2Ex(1-x)/(k_\perp^2 + x^2M^2)$ is the formation time of the radiated gluons. $\hat{q} = q_0(T/T_0)^3 p_\mu u^\mu$ is the jet transport parameter, where $q_0 = 1.5\ {\rm GeV}^2/{\rm fm}$, $u^\mu$ is the local velocity of the QGP, and $T_0$ is the initial temperature. The jet transport parameter is used to control the magnitude of energy loss due to jet-medium interaction. The number of radiated gluons is sampled from a Poisson distribution during each inelastic scattering.

$$P(n_g,t,\Delta t) = \frac{\langle N(t,\Delta t)\rangle^{n_g}}{n_g!}{\rm e}^{-\langle N(t,\Delta t)\rangle}. \tag{5}$$

In our calculation, $P_{\rm rad}(t,\Delta t)$ is initially evaluated to determine whether the radiation happens during $\Delta t$. If accepted, the Possion distribution $P(n_g,t,\Delta t)$ is used to sample the number of radiated gluons. Finally, the energy fraction ($x$) and transverse momentum ($k_\perp$) of the radiated gluon is sampled based on the spectrum shown in Eq. (4).

To calculate the collisional energy loss of these showered partons, a Hard Thermal Loop (HTL) formula [117] is adopted in the study: $\frac{{\rm d}E^{\rm coll}}{{\rm d}t} = \frac{\alpha_s C_s \mu_D^2}{2}\ln\frac{\sqrt{ET}}{\mu_D}$. The space-time evolution of the expanding fireball is given by the CLVisc hydrodynamic model [118]. When local temperature falls below $T_c = 165$ MeV, all the showered partons stop their propagation in the QGP medium and fragment into hadrons. In this work, we first construct strings using the colorless method developed by the JETSCAPE collaboration [119] and then perform hadronization and hadron decays using the PYTHIA Lund string method.

We also include the medium response effect in the calculation by considering that the lost energy in the collisional process is deposited into the evolved QGP medium. This deposited energy disturbs the medium, exciting a hydrodynamic wake correlated with the parton's direction. Following freeze-out, this wake hadronizes and produces soft hadrons that can be reconstructed within the jet cone. To incorporate this medium response effect, we employ a hybrid approach based on the Cooper-Frye freeze-out prescription with perturbations [39, 120]. The resulting distribution of wake particles is given by

$$E\frac{{\rm d}\Delta N}{{\rm d}^3p} = \frac{1}{32\pi}\frac{m_{\rm T}}{T^5}\cosh(y-y_j)\exp\left[-\frac{m_{\rm T}}{T}\cosh(y-y_j)\right] \times\left\{p_T\Delta P_{\rm T}\cos(\phi-\phi_j)+\frac{1}{3}m_{\rm T}\Delta M_{\rm T}\cosh(y-y_j)\right\}. \tag{6}$$

Here, $m_{\rm T}$, $p_{\rm T}$, $y$, and $\phi$ denote the transverse mass, transverse momentum, rapidity, and azimuthal angle of the emitted wake hadrons, respectively. The variables $y_j$ and $\phi_j$ denote rapidity and azimuthal angle of the initiating energetic parton. $T$ denotes the freeze-out temperature of the hot QCD medium. $\Delta M_{\rm T} = \Delta E/\cosh(y_j)$ and $\Delta P_{\rm T}$ denote the transverse mass and transverse momentum transferred from the jet to the medium, where $\Delta E$ denotes the deposited energy.

### B. Collisional vs. radiative vs. medium response

The angular distribution of the EEC within a jet inherently reflects medium-induced modifications of jet constituents and offers a direct connection to the scale and structure of the QGP. This distribution can be used to explore jet-induced medium response, medium-induced radiation, and transverse momentum broadening. We calculate the distributions as functions of $R_{\rm L}$ for inclusive charged jets in Pb+Pb collisions at $\sqrt{s} = 5.02$ TeV to predict the possible ALICE measurement. Fig. 3 shows the A+A/p+p ratio of the $\Sigma_{\rm EEC}$ distributions as functions of $R_{\rm L}$ with the jet radius of $R = 0.4$ in the jet $p_{\rm T}$ interval of $40-60$ GeV shown in the solid blue line. Clear enhancements are observed at $R_{\rm L} > 0.3$ and $R_{\rm L} < 0.06$ along with suppression at $R_{\rm L}$ of approximately $0.06-0.3$. From the distribution shifting point of view, it implies there are shifts toward larger $R_{\rm L}$ and smaller $R_{\rm L}$ at the same time. There have to be two effects competing with each other. To isolate the contributions and effects from different jet quenching mechanisms, we also plot in the same figure the A+A/p+p ratios as functions of $R_{\rm L}$: only considering radiative energy loss, denoted as the dashed dotted line; only considering collisional energy loss, denoted as the dotted line; considering both collisional and radiative energy loss but excluding medium response effect, denoted as the dashed line. We will apply the same notation in the following discussion.

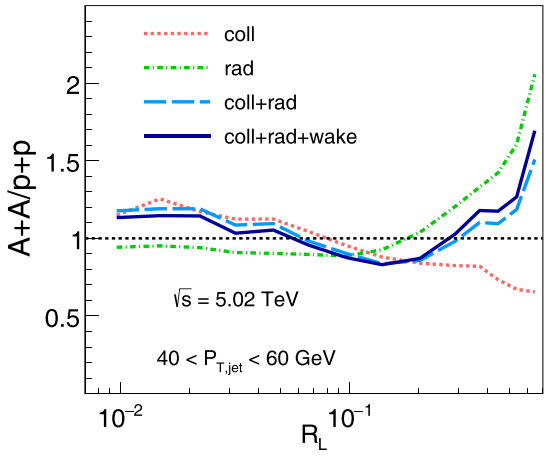


**Fig. 3.** (color online) A+A/p+p ratios of the $\Sigma_{EEC}$ distributions as functions of $R_L$ for inclusive charged jets with a radius of $R = 0.4$ in central (0−10%) Pb + Pb collisions at $\sqrt{s} = 5.02$ TeV in jet $p_T$ interval 40 – 60 GeV calculated considering four scenarios of jet quenching mechanism: collisional energy loss, radiative energy loss, collisional+radiative energy loss and collisional+radiative energy loss+medium response.

First, we find that the pure collisional energy loss process leads to a gradual enhancement in the smaller $R_L$ region and a gradual suppression in the larger $R_L$ region, indicating that the energy loss mechanism, which does not alter the particle propagation direction, results in a concentration of the energy weight distribution toward smaller $R_L$ values. Second, the pure radiative energy loss process leads to a rapid enhancement with increasing $R_L$ in $R_L > 0.2$ and a slight suppression at $R_L < 0.2$, indicating a clear broadening effect toward larger $R_L$ values in the distribution. It is a typical consequence of the medium-induced gluon radiation. The final A+A/p+p ratio is almost exactly the result of the competition of the two mechanisms. The medium response effect is visible and mild in this specific observable, but it has the same diffusion behavior of enhancing the distribution in the larger $R_L$ values and suppressing that in the smaller $R_L$ region as the radiative energy loss process.

To gain deeper insight into the physical implications of this result, we examine the theoretical predictions from the following three perspectives: probing finer jet substructures revealed by the EEC observable itself, specifically the distribution of average paired-energy weight versus $R_L$ shown in Fig. 2; impact of selection bias, which is a common effect in jet substructure observables, on the EEC measurements; capability of this observable to distinguish quark-initiated jets from gluon-initiated jets in jet quenching, along with the underlying mechanisms for these differences.

### C. In-jet finer substructure as revealed by the EEC

By applying the strategy discussed in Eq. (2) and Fig. 2, we first calculate the ratio of the $R_L$-distribution of paired-particle counts normalized to the number of jets in Pb + Pb collisions to that in p + p collisions shown in the upper panel of Fig. 4. Elastic energy loss leads to a reduction in the $R_L$-distribution of paired-energy counts in A+A compared to the p+p case, and this reduction becomes more pronounced with increasing $R_L$. The overall suppression demonstrates a reduction in the number of particle pairs. The slope of the curve indicates that it leads to an enhancement of the distribution in the small $R_L$ region relative to that in the large $R_L$ region. The dashed-dotted line demonstrates that radiative energy loss causes the $R_L$-distribution of paired-energy counts for jets in A+A collisions to shift towards larger $R_L$. The dashed line shows the competition between two mechanisms. The comparison between the total effect represented by the solid line and dashed line reveals that the effect of medium response on the $R_L$-distribution of paired-particle counts is manifested as an enhancement in the large $R_L$ region. Furthermore, the medium response resulting in an increase in the number of jet constituents contributes en-

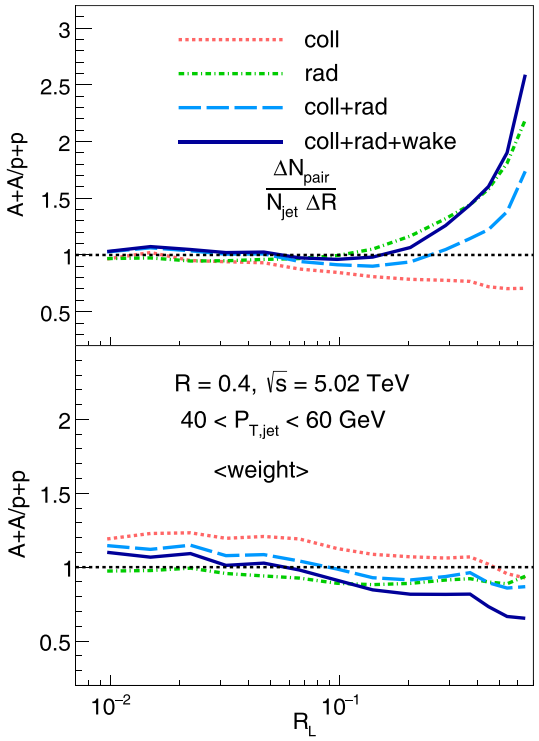


**Fig. 4.** (color online) Ratio of the $R_L$ distribution of paired-particle counts normalized to the number of jets in Pb + Pb collisions to that in p + p collisions (upper panel) and the ratio the $R_L$-distribution of averaged energy-energy weight in Pb + Pb collisions to that in p + p collisions (lower panel) for inclusive charged jets with the size of $R = 0.4$ in the jet transverse momentum interval of $40\ \text{GeV} < p_{T,\text{jet}} < 60$ GeV produced at $\sqrt{s} = 5.02$ TeV. The results of the four jet quenching scenarios are also plotted same way as in Fig. 3.

tirely to the distribution in this specific region.

From the bottom panel of Fig. 4, we observe that all types of jet quenching mechanisms lead to an elevation of the averaged energy-energy weights (⟨weight⟩s) in the small $R_L$ region relative to those in the large $R_L$ region. This behavior explains why the A+A/p+p ratio of the EEC shown in Fig. 3 exhibits an enhancement in the small $R_L$ region, while its rise, when moving towards the large $R_L$ region, is weaker than that observed in the paired-particle count distribution in the upper panel. The ratio value obtained from radiative energy loss is lower than that from collisional energy loss because radiative energy loss increases the number of particle pairs, whereas collisional energy loss reduces it. The inclusion of the medium response effect, due to the resulting increase in the number of jet constituents, causes a reduction in the ⟨weight⟩s. This creates a stark contrast to the sharp rise it induces in the paired-particle count distribution within the large $R_L$ region, leading to a mild overall effect of the medium response to the A+A/p+p ratio of EEC. Therefore, we find that the upper and lower parts shown in the figure exhibit exactly opposite trends in their response to changes in the number of jet constituents, resulting in a partial cancellation effect.

### D. Quark-initiated jets versus gluon-initiated jets

Nonetheless, we need to examine the reason why the ⟨weight⟩ distribution in A+A collisions is relatively more concentrated towards the small $R_L$ region. As suggested by the jet-$p_T$ dependence of the EEC distribution shown in Fig. 1, this phenomenon may be attributed to selection bias. However, does this imply that energy loss mechanisms cannot drive the ⟨weight⟩ towards larger $R_L$ angles? Is this phenomenon consistent for both quark- and gluon-initiated jets? We find that a comprehensive understanding of flavor-dependent jet-quenching effects on the EEC observable remains elusive. To address this gap, we intend to conduct further discussion focusing on the following aspects: initial p+p production, different jet quenching mechanisms, in-jet finer substructure as revealed by the EEC, selection bias effect, and flavor-dependent attribution. We begin our discussion by comparing purely quark-initiated jets and purely gluon-initiated jets generated by PYTHIA.

***Initial p+p production*** - Given the experimental challenge of identifying or defining quark versus gluon-initiated jets, we adopt a simulation-based approach. Using PYTHIA 8, we generate events from hard processes constrained to produce exclusively quarks or exclusively gluons. Jets are then reconstructed in these events and used for our case study.

In Fig. 5 we plot $\Sigma_{EEC}$ distributions as functions of $R_L$ for inclusive charged jets, pure gluon-initiated and quark -initiated jets with a size of $R = 0.4$ in the jet transverse momentum interval of $40\ \text{GeV} < p_{T,jet} < 60\ \text{GeV}$ produced in $p+p$ collisions at $\sqrt{s} = 5.02$ TeV simultaneously. We observe that gluon-initiated jets peak around $R_L = 0.08$, while quark-initiated jets exhibit higher distribution values and are more concentrated in the small-$R_L$ region. Inclusive charged jets represent a mixture of the two, and their distribution closely resembles that of gluon-initiated jets. Furthermore, this observation reveals that within this kinematic regime, the charged-hadron jet sample is predominantly dominated by gluon-initiated jets. The transition from gluon-initiated to quark-initiated jets produces an effect similar to what is achieved by increasing the jet $p_T$.

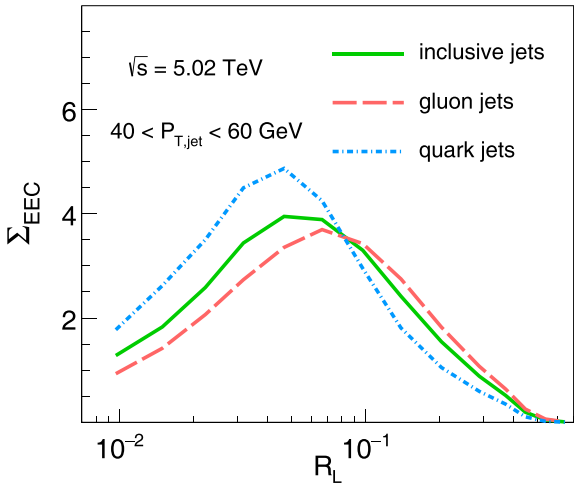


**Fig. 5.** (color online) PYTHIA8 simulation results of defined $\Sigma_{EEC}$ distributions as functions of $R_L$ for inclusive charged jets, pure gluon-initiated jets and quark -initiated jets with a jet size of $R = 0.4$ in the jet transverse momentum interval of $40\ \text{GeV} < p_{T,jet} < 60\ \text{GeV}$ produced in $p+p$ collisions at $\sqrt{s} = 5.02$ TeV.

***Different jet quenching mechanism*** - In Fig. 6, within the same kinematic regime, the jet quenching patterns for different flavor-initiated jets are individually investigated. First, we present the A+A/p+p ratios of the $\Sigma_{EEC}$ distributions for quark-initiated jets and gluon-initiated jets in the upper and lower panels, respectively. Below $R_L = 0.15$, a slight and gradual suppression is observed for quark-initiated jets in the upper panel, whereas beyond $R_L = 0.15$, the ratio exhibits an increasing behavior with rising $R_L$. The enhancement observed in the large-$R_L$ region reveals a distinct diffusion effect induced by jet quenching for quark-initiated jets. However, the suppression seen in the small-$R_L$ region indicates that the selection bias effect is not manifested. In the lower panel, we observe a significant enhancement for gluon-initiated jets in the small-$R_L$ region below 0.07. This enhancement becomes more pronounced as $R_L$ decreases. Additionally, a substantial increase is also observed in the large-$R_L$ re-

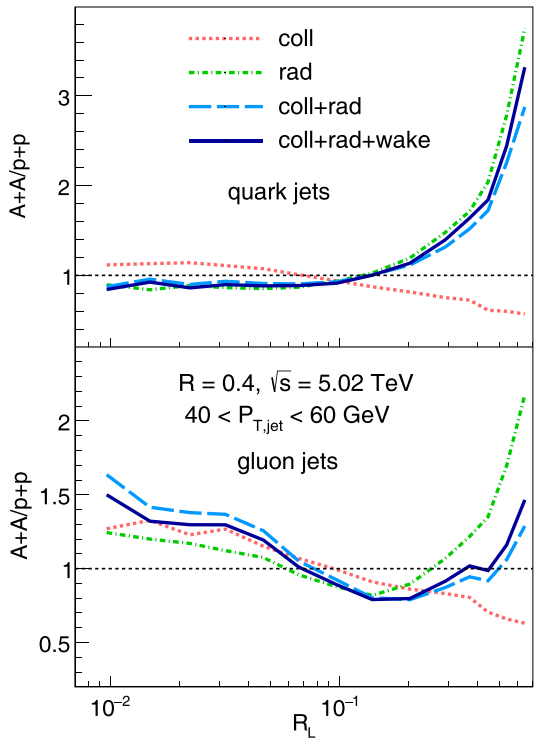


**Fig. 6.** (color online) A+A/p+p ratios of the $\Sigma_{EEC}$ distributions for quark-initiated jets (upper panel) and gluon-initiated jets (bottom panel) separately calculated in the four jet quenching scenarios plotted in the same manner and the same kinetic region as in Fig. 3.

gion beyond 0.4, where the ratio rises monotonically with increasing $R_L$.

Figure 1 indicates that jets with higher transverse momentum tend to populate the distribution in the smaller-$R_L$ region. The enhancement observed in the small-$R_L$ region in this figure likely originates from contributions of higher-$p_T$ jets before significant energy loss occurs. Notably, quark- and gluon-initiated jets exhibit significantly distinct responses to this mechanism. This difference may partly be explained by examining Fig. 5: quark-initiated jets predominantly distribute in intrinsically smaller $R_L$ regions, whereas gluon-initiated jets favor larger $R_L$ regions. Furthermore, in the large-$R_L$ region, the observed enhancement is smaller for gluon jets than for quark jets. These characteristic differences collectively constitute the discriminatory power of the EEC observable in distinguishing the jet quenching signatures of quark-initiated versus gluon-initiated jets.

Simultaneously, we also compute the isolated impact of different jet quenching mechanisms on their respective A+A/p+p ratios, shown alongside the curve representing the overall consideration of the jet quenching mechanisms, following the methodology employed in Fig. 3. For the pure elastic energy loss mechanism, we find that regardless of gluon-initiated or quark-initiated jets, enhancement in the small-$R_L$ region and suppression in the large-$R_L$ region are consistently observed. This tends to increase their relative weighting at small $R_L$. However, the effect is less pronounced for quark-initiated jets when compared to gluon-initiated jets, noting that quark jets already exhibit a stronger tendency to populate the small-$R_L$ region than gluon jets. By contrast, the radiative energy loss mechanism exhibits significantly greater differences between quark-jets and gluon-jets than elastic energy loss. For quark-initiated jets, radiative energy loss manifests as suppression in the small-$R_L$ region and enhancement in the large-$R_L$ region. Its behavior almost entirely dictates the overall A+A/p+p ratio pattern, rendering the contribution from elastic energy loss negligible. The medium response effect provides only a minor enhancing contribution in the large $R_L$ region. This effect arises because medium excitations produced by energy deposition from the jet are preferentially emitted away from the jet axis, resulting in weaker correlations with the jet constituents. For gluon-initiated jets, radiative energy loss manifests as an enhancement in the small and large $R_L$ regions. Overall, radiative energy loss still dominates the A+A/p+p ratio for gluon jets. However, its dominance is more substantially diminished by the opposing effects of elastic energy loss when compared to the case in quark-initiated jets, where it holds a stronger position.

***Selection bias effect*** - Through the aforementioned analysis and comparisons, we recognize the critical need to further characterize the selection bias effects experienced separately by quark- and gluon-initiated jets, moving beyond intuitive interpretations based solely on the $p_T$-dependence observed in Fig. 1. We employ the following methodology: Jets with reconstructed transverse momentum in the 40 – 60 GeV range in A+A collisions are categorized into two classes: *Falldown*, jets originating from partons that, prior to energy loss, would have produced jets with $p_T > 60$ GeV in the corresponding p+p collisions. *Survival*, jets originating from partons that, before energy loss, would have produced jets with $p_T$ in the 40 – 60 GeV range in the corresponding p+p collisions. In Fig. 7, we compare the A+A/p+p ratios of the EEC distributions for quark-initiated and gluon-initiated jets, separately showing the contributions originating from the *Falldown* and *Survival* components for each flavor.

We observe that the energy loss patterns manifested by the *Falldown* and *Survival* components are dynamically analogous. The characteristic differences in energy loss signatures fundamentally originate from the flavor of the initial partons. Comparatively, the *Falldown* contribution consistently exhibits a stronger enhancing effect in the small-$R_L$ region while producing relatively weaker diffusion in the large-$R_L$ region. The combined effect observed in Fig. 3 arises from the mixture of these *Falldown* and *Survival* components. Examining the *Survival*

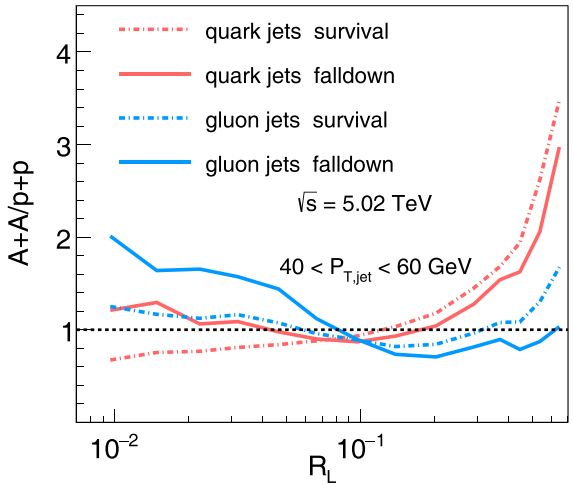


**Fig. 7.** (color online) A+A/p+p ratios for EEC distributions as a function of $R_{\rm L}$ for quark- and gluon-initiated jets with two categories: *Survival* and *Falldown* in central (0−10%) Pb+Pb collisions at $\sqrt{s}=5.02$ TeV in jet $p_{\rm T}$ interval $40-60$ GeV.

component in isolation reveals that in the small-$R_{\rm L}$ region, even without the amplified selection bias effect intrinsic to the *Falldown* population, gluon-initiated jets inherently generate a slight enhancement due to their characteristic energy loss pattern. The selection bias effect further augments this enhancement. Simultaneously, we note that the enhancing effect of selection bias in this region remains insufficient to counteract the suppressing effect of quark jet energy loss. This leads to the empirical observation that gluon jets appear more susceptible to selection bias. The underlying physics, however, indicates that quark and gluon jets experience selection bias. The observed difference primarily arises from the flavor-dependent characteristics of energy loss imprinted on the EEC observable.

***In-jet finer substructure of EEC*** - To gain further insight into the aforementioned differences in jet quenching effects between quark- and gluon-initiated jets through the substructure details revealed by the EEC, we present the following in Fig. 8. Upper panels: the A+A/p+p ratios of the normalized paired-particle count $R_{\rm L}$ distributions (normalized per jet) for quark-initiated jets (left) and gluon-initiated jets (right). Lower panels: the A+A/p+p ratios of the ⟨weight⟩s $R_{\rm L}$ distributions for quark-initiated jets (left) and gluon-initiated jets (right). Additionally, results showing the isolated effects of different jet quenching mechanisms are overlaid in each panel.

Let's commence with the A+A/p+p ratios of the normalized paired-particle count $R_{\rm L}$ distributions. For quark-initiated jets: The angular distribution of paired particles diffuses toward larger $R_{\rm L}$ values. Elastic energy loss suppresses this trend by inducing suppression at large $R_{\rm L}$, but

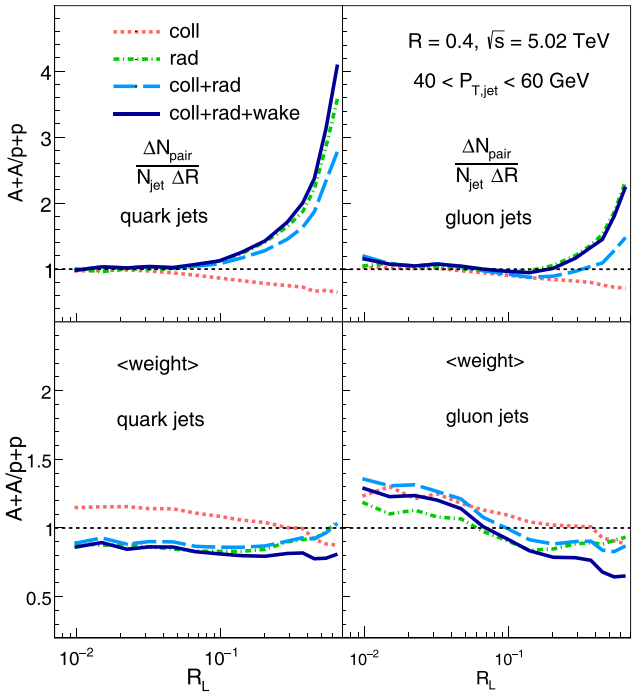


**Fig. 8.** (color online) A+A/p+p ratios of the number of jets normalized paired-particle count $R_{\rm L}$ distributions for quark-initiated jets (left) and gluon-initiated jets (right) are plotted in the upper panels; A+A/p+p ratios of the ⟨weight⟩s $R_{\rm L}$ distributions for quark-initiated jets (left) and gluon-initiated jets (right) are plotted in the lower panels. The jets are with a jet size of $R=0.4$ in the jet transverse momentum interval of $40\ {\rm GeV} < p_{\rm T,jet} < 60$ GeV produced in Pb+Pb collisions at $\sqrt{s}=5.02$ TeV.

the medium response effect compensates for this suppression. Consequently, the net effect nearly matches that of radiative energy loss. For gluon-initiated jets: The physical behavior pattern is analogous, although the diffusion toward larger $R_{\rm L}$ occurs to a lesser extent than in quark jets.

Turning now to the A+A/p+p ratios of the ⟨weight⟩ $R_{\rm L}$ distributions: for quark-initiated jets, modifications to the ⟨weight⟩ are relatively mild overall. A slight enhancement only begins to emerge beyond $R_{\rm L}=0.3$. Furthermore, the entire modification remains dominated by radiative energy loss, even though the elastic energy loss mechanism exhibits opposing behavior, which is consistent with the indication from the upper panel. Similarly, we observe that the medium response effect provides a significant suppressing contribution in the large-$R_{\rm L}$ region, directly counteracting the enhancement induced by radiative energy loss. Consequently, this results in an overall gentle modification, suggesting that the ⟨weight⟩ distribution experiences no significant shift across the entire $R_{\rm L}$ range. For gluon-initiated jets, the shift of the ⟨weight⟩ toward the concentration in the small-$R_{\rm L}$ region is significantly pronounced. Loss of radiative and elastic

energies contribute in the same direction (toward this shift), and the medium response effect further suppresses the distribution in the large-$R_L$ region.

Building on the two refined aspects of jet substructure quenching effects, we now analyze the results in Fig. 6, which reflect their combined impact. For quark-initiated jets, elastic energy loss contributes negligibly. Radiative energy loss and medium response increase the number of jet constituents. This significantly enhances the paired-particle count $R_L$ distribution while substantially suppressing the ⟨weight⟩. In the small-$R_L$ region, minimal modification to paired-particle counts dominates. The suppression of ⟨weight⟩ thus causes an overall suppression in the total EEC A+A/p+p ratio. In the large-$R_L$ region, the strong enhancement in paired-particle counts is partially counteracted by suppressed ⟨weight⟩. Nevertheless, a significant net enhancement persists. For gluon-initiated jets, the enhancement in the paired-particle count $R_L$ distribution is weaker than in quark jets. The critical difference lies in modifications to the ⟨weight⟩ $R_L$ distribution: in the small $R_L$ region, an enhancement is observed; in the large $R_L$ region, pronounced suppression is observed. Consequently, enhanced ⟨weight⟩ drives an overall enhancement in the total EEC A+A/p+p ratio in the small-$R_L$ region, while suppression of ⟨weight⟩ further diminishes the enhancement of the paired-particle counts in the large-$R_L$ region.

## IV. ATTRIBUTION AND SUMMARY

We analyzed the differences in A+A/p+p $R_L$ distributions between quark and gluon jets through four distinct dimensions: initial production mechanisms, variations in jet quenching mechanisms, internal substructure details revealed by EEC, and differential susceptibility to selection bias. We now investigate the fundamental origins of the flavor-dependent jet quenching effects observed in the EEC.

We therefore compute the A+A/p+p ratios of the EEC distributions under two counterfactual scenarios: pure gluon jets traversing the medium with quark-like energy loss characteristics, and pure quark jets subjected to gluon-like energy loss dynamics. Results are presented in Fig. 9. These variations arise not only from differences in the interaction strength between quarks/gluons and the hot and dense medium but also from distinct radiation patterns of gluons in radiative energy loss. We quantify this impact by highlighting the variation range between the nominal A+A/p+p ratio and our counterfactual ratio through shaded bands in the figure. For gluon jets with suppressed energy loss, we observe the expected attenuation of energy loss and selection bias effects. However, enhancements persist across small and large $R_L$ regions. Conversely, enhancing quark energy loss to gluon-like levels dramatically amplifies the EEC distribution in

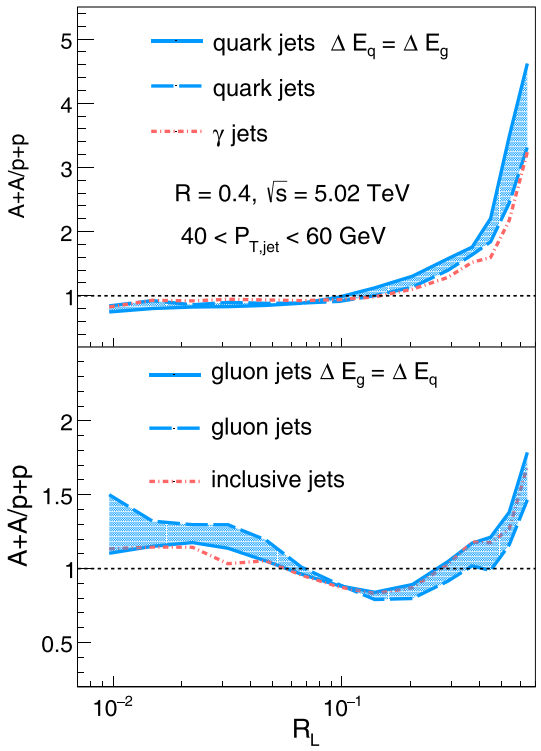


**Fig. 9.** (color online) Counterfactual analysis of flavor-dependent jet quenching via EEC distributions. (upper) Quark jets with energy loss equivalent to gluon jets ($\Delta E_q = \Delta E_g$), compared to $\gamma$-tagged quark jets under standard quenching. (lower) Gluon jets with energy loss equivalent to quark jets ($\Delta E_g = \Delta E_q$), compared to inclusive jets under standard quenching. All jets reconstructed with $R = 0.4$ in central (0−10%) Pb+Pb collisions at $\sqrt{s_{NN}} = 5.02$ TeV with transverse momentum $40 < p_{T,jet} < 60$ GeV. Shaded bands indicate the variation range between nominal and counterfactual A+A/p+p ratios.

A+A collisions at large $R_L$ while preserving the characteristic suppression at small $R_L$.

Consequently, the characteristic differences in the A+A/ p+p ratios of EEC distributions between quark- and gluon-initiated jets primarily stem from pre-quenching distribution disparities, not from flavor-dependent energy loss mechanisms, and crucially not from divergent gluon radiation patterns during radiative energy loss.

To experimentally observe and utilize this flavor-dependent difference, we propose photon-tagged jets as proxies for quark-initiated jets and inclusive charged-hadron jets within the same kinematic regime as proxies for gluon-initiated jets. We compare the photon-tagged jets and pure quark-initiated jets in the upper panel. The A+A/p+p ratios of EEC distributions for both jet types are compared within the same kinematic window. The photon-tagged jet results show notably closer alignment with unmodified quark-initiated jets. The inclusive charged-hadron jets are compared to pure gluon-initiated

jets in the lower panel. The results for inclusive charged-hadron jets align closely with those of gluon-initiated jets, which have been artificially modified to undergo quark-like energy loss.

In summary, through PYTHIA simulations validated against ALICE p+p data and an improved SHELL model incorporating collisional/radiative energy loss in addition to medium response, we systematically quantify flavor-dependent jet quenching via energy-energy correlators (EEC) in $\sqrt{s_{NN}} = 5.02$ TeV Pb+Pb collisions. Key findings include that the flavor-dependent quenching signatures in this study are characterized by pure quark jets exhibiting a strong enhancement at $R_{\rm L} > 0.2$, and gluon jets displaying a bimodal enhancement at small ($R_{\rm L} < 0.07$) and large ($R_{\rm L} > 0.4$) angular scales. Dual-shift decomposition is illustrated in the A+A/p+p ratio of the EEC, where shifts toward large $R_{\rm L}$ ($> 0.3$) primarily stem from energy loss effects. Shifts toward small $R_{\rm L}$ ($< 0.06$) are not fully attributable to selection bias. Counterfactual analysis reveals that intrinsic gluon jet enhancement is also evident in small- $R_{\rm L}$ regions. The aspect of the substructure-resolved discrimination is that the quark jets suffer global suppression of $\langle{\rm weight}\rangle(R_{\rm L})$ and gluon jets suffer concentration of $\langle{\rm weight}\rangle$ toward small $R_{\rm L}$. Based on the mechanism decomposition point of view, elastic energy loss concentrates $\langle{\rm weight}\rangle(R_{\rm L})$ toward small $R_{\rm L}$, radiative energy loss dominates quark jet modifications, and medium response amplifies large $R_{\rm L}$ enhancement via soft hadron production. These results indicate that flavor dependence in EEC modifications is predominantly driven by intrinsic gluon/quark-initiated jet distribution structure differences rather than medium-induced mechanisms. At the end of the manuscript, we propose photon-tagged jets as proxies for quarks and inclusive charged-hadron jets as proxies for gluons. $\gamma$-tagged jets reproduce the pure quark jet quenching signatures, and inclusive jets exhibit gluon-like behavior when subjected to quark-like energy loss. These results establish the EEC as a precision probe of color-charge-dependent jet-medium interactions, providing new constraints for $\hat{q}$ extraction and QGP tomography. Meanwhile, the dominant role of initial jet structure suggests that future analyses must account for pre-quenching flavor asymmetries.

## References


[1] M. Gyulassy and M. Plumer, Phys. Lett. B **243**, 432 (1990)
[2] X. F. Luo and N. Xu, Nucl. Sci. Tech. **28**(8), 112 (2017)
[3] Z. B. Tang, W. M. Zha, W. M. Zha *et al.*, Nucl. Sci. Tech. **31**(8), 81 (2020)
[4] H. X. Zhang, Y. X. Xiao, J. W. Kang *et al.*, Nucl. Sci. Tech. **33**(11), 150 (2022)
[5] Q. Y. Shou, Y. G. Ma, S. Zhang *et al.*, Nucl. Sci. Tech. **35**(12), 219 (2024)
[6] X. N. Wang and M. Gyulassy, Phys. Rev. Lett. **68**, 1480 (1992)
[7] M. Gyulassy, I. Vitev, X. N. Wang *et al.*, *Jet quenching and radiative energy loss in dense nuclear matter*, p 123–191, (2004)
[8] G. Y. Qin and X. N. Wang, Int. J. Mod. Phys. E **24**(11), 1530014 (2015)
[9] C. Young, B. Schenke, S. Jeon *et al.*, Phys. Rev. C **84**, 024907 (2011)
[10] Y. C. He, I. Vitev, and B. W. Zhang, Phys. Lett. B **713**, 224 (2012)
[11] R. B. Neufeld, I. Vitev, and B. W. Zhang, Phys. Rev. C **83**, 034902 (2011)
[12] K. C. Zapp, F. Krauss, and U. A. Wiedemann, JHEP **03**, 080 (2013)
[13] W. Dai, I. Vitev, and B. W. Zhang, Phys. Rev. Lett. **110**(14), 142001 (2013)
[14] G. L. Ma, Phys. Rev. C **87**(6), 064901 (2013)
[15] F. Senzel, O. Fochler, J. Uphoff *et al.*, J. Phys. G **42**(11), 115104 (2015)
[16] J. Casalderrey-Solana, D. C. Gulhan, J. G. Milhano *et al.*, JHEP, **10**, 019 (2014) [Erratum: JHEP **09**, 175 (2015)]
[17] J. G. Milhano and K. C. Zapp, Eur. Phys. J. C **76**(5), 288 (2016)
[18] N. B. Chang and G. Y. Qin, Phys. Rev. C **94**(2), 024902 (2016)
[19] A. Majumder and J. Putschke, Phys. Rev. C **93**(5), 054909 (2016)
[20] L. Chen, G. Y. Qin, S. Y. Wei *et al.*, Phys. Lett. B **782**, 773 (2018)
[21] Y. T. Chien and I. Vitev, Phys. Rev. Lett. **119**(11), 112301 (2017)
[22] L. Apolinário, J. G. Milhano, M. P.loskon *et al.*, Eur. Phys. J. C **78**(6), 529 (2018)
[23] M. Connors, C. Nattrass, R. Reed *et al.*, Rev. Mod. Phys. **90**, 025005 (2018)
[24] S. L. Zhang, T. Luo, X. N. Wang *et al.*, Phys. Rev. C **98**, 021901 (2018)
[25] W. Dai, S. Wang, S. L. Zhang *et al.*, Chin. Phys. C **44**, 104105 (2020)
[26] T. Luo, S. S. Cao, Y. Y. He *et al.*, Phys. Lett. B **782**, 707 (2018)
[27] N. B. Chang, Y. Tachibana, and G. Y. Qin, Phys. Lett. B **801**, 135181 (2020)
[28] S. Wang, W. Dai, B. W. Zhang *et al.*, Eur. Phys. J. C **79**(9), 789 (2019)
[29] S. Y. Chen, B. W. Zhang, and E. K. Wang, Chin. Phys. C **44**(2), 024103 (2020)
[30] L. Chen, S. Y. Wei, and H. Z. Zhang, Eur. Phys. J. C **80**(12), 1136 (2020)
[31] S. Wang, W. Dai, B. W. Zhang *et al.*, Chin. Phys. C **47**(5), 054102 (2023)
[32] J. Yan, S. Y. Chen, W. Dai *et al.*, Chin. Phys. C **45**(2), 024102 (2021)
[33] S. Wang, W. Dai, B. W. Zhang *et al.*, Chin. Phys. C **45**(6), 064105 (2021)
[34] S. L. Zhang, M. Q. Yang, and B. W. Zhang, Eur. Phys. J. C **82**(5), 414 (2022)
[35] Y. Li, S. W. Shen, S. Wang *et al.*, Nucl. Sci. Tech. **35**(7), 113 (2024)

[36] Y. T. Chien and I. Vitev, JHEP **05**, 023 (2016)
[37] A. M. Sirunyan *et al.* (CMS Collaboration), Phys. Rev. Lett. **122**(15), 152001 (2019)
[38] Z. Yang, T. Luo, W. Chen *et al.*, Phys. Rev. Lett. **130**(5), 052301 (2023)
[39] J. Casalderrey-Solana, D. Gulhan, G. Milhano *et al.*, JHEP **03**, 135 (2017)
[40] A. M. Sirunyan *et al.* (CMS Collaboration), Phys. Rev. Lett. **121**(24), 242301 (2018)
[41] M. Aaboud *et al.* (ATLAS Collaboration), Phys. Rev. C **98**(2), 024908 (2018)
[42] W. Chen, S. S. Cao, T. Luo *et al.*, Phys. Lett. B **810**, 135783 (2020)
[43] S. Acharya *et al.* (A Large Ion Collider Experiment and ALICE Collaborations), Phys. Rev. Lett. **128**(10), 102001 (2022)
[44] C. L. Basham, L. S. Brown, S. D. Ellis *et al.*, Phys. Rev. D **17**, 2298 (1978)
[45] C. L. Basham, L. S. Brown, S. D. Ellis *et al.*, Phys. Rev. Lett. **41**, 1585 (1978)
[46] C. L. Basham, L. S. Brown, S. D. Ellis *et al.*, Phys. Rev. D **19**, 2018 (1979)
[47] C. Berger *et al.* (PLUTO Collaboration), Z. Phys. C **28**, 365 (1985)
[48] A. J. Larkoski, G. P. Salam, and J. Thaler, JHEP **06**, 108 (2013)
[49] A. J. Larkoski and I. Moult, Phys. Rev. D **93**, 014017 (2016)
[50] L. J. Dixon, M. X. Luo, V. Shtabovenko *et al.*, Phys. Rev. Lett. **120**(10), 102001 (2018)
[51] H. Chen, M. X. Luo, I. Moult *et al.*, JHEP **08**, 028 (2020)
[52] J. M. Henn, E. Sokatchev, K. Yan *et al.*, Phys. Rev. D **100**(3), 036010 (2019)
[53] H. Chen, I. Moult, X. Y. Zhang *et al.*, Phys. Rev. D **102**(5), 054012 (2020)
[54] J. Gao, V. Shtabovenko, and T. Z. Yang, JHEP **02**, 210 (2021)
[55] H. T. Li, Y. Makris, and I. Vitev, Phys. Rev. D **103**(9), 094005 (2021)
[56] P. T. Komiske, I. Moult, J. Thaler *et al.*, Phys. Rev. Lett. **130**(5), 051901 (2023)
[57] D. Neill, G. Vita, I. Vitev *et al.*, Energy-Energy Correlators for Precision QCD. In *Snowmass 2021*, 3, (2022)
[58] X. h. Liu and H. X. Zhu, Phys. Rev. Lett. **130**(9), 091901 (2023)
[59] H. Chen, I. Moult, J. Thaler *et al.*, JHEP **07**, 146 (2022)
[60] J. Holguin, I. Moult, A. Pathak *et al.*, Phys. Rev. D **107**(11), 114002 (2023)
[61] K. Lee, B. Meçaj, and I. Moult, Phys. Rev. D **111**(1), L011502 (2025)
[62] H. Y. Liu, X. h. Liu, J. C. Pan *et al.*, Phys. Rev. Lett. **130**(18), 181901 (2023)
[63] H. t. Cao, X. h. Liu, and H. X. Zhu, Phys. Rev. D **107**(11), 114008 (2023)
[64] W. Chen, J. Gao, Y. b. Li *et al.*, JHEP **05**, 043 (2024)
[65] M. Jaarsma, Y. b. Li, I. Moult *et al.*, JHEP **12**, 087 (2023)
[66] K. Lee and I. Moult, *Energy Correlators Taking Charge*, 8, (2023)
[67] Z. B. Kang, K. Lee, D. Y. Shao *et al.*, JHEP **03**, 153 (2024)
[68] Z. B. Kang, K. Lee, D. Y. Shao *et al.*, Collins-type Energy-Energy Correlators and Nucleon Structure. In *30th International Workshop on Deep-Inelastic Scattering and Related Subjects*, 7, (2023)
[69] A. P. Chen, X. h. Liu, and Y. Q. Ma, Phys. Rev. Lett. **133**, 191901 (2024)
[70] J. Barata, J. G. Milhano, and A. V. Sadofyev, Eur. Phys. J. C **84**(2), 174 (2024)
[71] J. Holguin, I. Moult, A. Pathak *et al.*, Phys. Rev. Lett. **134**(23), 231903 (2025)
[72] J. Barata and R. Szafron, Phys. Rev. D **110**(3), L031501 (2024)
[73] S. Alipour-fard and W. J. Waalewijn, *Energy Correlators Beyond Angles,* 1, (2025)
[74] E. Craft, K. Lee, B. Meçaj *et al.*, *Beautiful and Charming Energy Correlators*, 10, (2022)
[75] C. Andres, F. Dominguez, R. K. Elayavalli *et al.*, Phys. Rev. Lett. **130**(26), 262301 (2023)
[76] C. Andres, F. Dominguez, J. Holguin *et al.*, JHEP **09**, 088 (2023)
[77] J. Barata and Y. Mehtar-Tani, PoS **HardProbes2023**, 145 (2024)
[78] J. Barata, P. Caucal, A. Soto-Ontoso *et al.*, JHEP **11**, 060 (2024)
[79] B. Singh and V. Vaidya, JHEP **06**, 071 (2025)
[80] C. Andres, F. Dominguez, J. Holguin *et al.*, Phys. Rev. D **110**(3), L031503 (2024)
[81] C. Andres, F. Dominguez, J. Holguin *et al.*, *Simple Scaling Laws for Energy Correlators in Nuclear Matter,* 11, (2024)
[82] C. Andres, F. Dominguez, J. Holguin *et al.*, JHEP **03**, 166 (2025)
[83] Z. Yang, Y. y. He, I. Moult *et al.*, Phys. Rev. Lett. **132**(1), 011901 (2024)
[84] H. Bossi, A. S. Kudinoor, I. Moult *et al.*, JHEP **12**, 073 (2024)
[85] W. J. Xing, S. s. Cao, G. Y. Qin *et al.*, Phys. Rev. Lett. **134**(5), 052301 (2025)
[86] J. Barata, M. V. Kuzmin, J. G. Milhano *et al.*, *Jet EEC aWAKEning: hydrodynamic response on the celestial sphere*, 12, (2024)
[87] K. Devereaux, W. q. Fan, W. y. Ke *et al.*, *Imaging Cold Nuclear Matter with Energy Correlators*, 3, (2023)
[88] Y. Fu, B. Müller, and C. Sirimanna, *Modification of the Jet Energy-Energy Correlator in Cold Nuclear Matter*, 11, (2024)
[89] J. Barata, Z. B. Kang, X. M. López *et al.*, *Energy-Energy Correlator for jet production in pp and pA collisions*, 11, (2024)
[90] C. Andres, J. Holguin, R. K. Elayavalli *et al.*, Phys. Rev. Lett. **134**(8), 082303 (2025)
[91] C. Andres and J. Holguin, *Minimizing Selection Bias in Inclusive Jets in Heavy-Ion Collisions with Energy Correlators*, 9, (2024)
[92] A. Tamis, PoS **HardProbes2023**, 175 (2024)
[93] The CMS Collaboration, *Energy-energy correlators from PbPb and pp collisions at 5.02 TeV*, (2024)
[94] S. Acharya *et al.* (ALICE Collaboration), arXiv: 2409.12687 [hep-ex]
[95] S. Acharya *et al.*, (ALICE Collaboration), arXiv: 2504.03431 [hep-ex]
[96] X. N. Wang, Phys. Rev. C **58**, 2321 (1998)
[97] R. Baier, Y. L. Dokshitzer, A. H. Mueller *et al.*, Nucl. Phys. B **484**, 265 (1997)
[98] X. N. Wang and X. f. Guo, Nucl. Phys. A **696**, 788 (2001)

[99] P. B. Arnold, G. D. Moore, and L. G. Yaffe, JHEP **11**, 001 (2000)
[100] M. Gyulassy, P. Levai, and I. Vitev, Nucl. Phys. B **594**, 371 (2001)
[101] H. T. Li and I. Vitev, Phys. Rev. D **101**, 076020 (2020)
[102] A. M. Sirunyan *et al*., JHEP **07**, 115 (2020)
[103] Y. T. Chien and R. K. Elayavalli, *Probing heavy ion collisions using quark and gluon jet substructure*, 3, (2018)
[104] T. Sjöstrand, S. Ask, J. R. Christiansen *et al*., Comput. Phys. Commun. **191**, 159 (2015)
[105] P. Skands, S. Carrazza, and J. Rojo, Eur. Phys. J. C **74**(8), 3024 (2014)
[106] M. Cacciari, G. P. Salam, and G. Soyez, JHEP **04**, 063 (2008)
[107] S. Y. Chen, J. Yan, W. Dai *et al*., Chin. Phys. C **46**(10), 104102 (2022)
[108] Y. F. Liu, W. Dai, B. W. Zhang *et al*.,,Chin. Phys. C **49**, 044108 (2025)
[109] Y. Li, S. Wang, and B. W. Zhang, Phys. Rev. C **108**(2), 024905 (2023)
[110] S. Wang, Y. Li, J. W. Kang *et al*., *Unveiling the jet angular broadening with γ-jet in high-energy nuclear collisions*, 8, (2024)
[111] Y. Li, S. Y. Chen, W. x. Kong *et al*., *Medium modifications of heavy-flavor jet angularities in high-energy nuclear collisions*, 9, (2024)
[112] B. Alver, M. Baker, C. Loizides *et al*., *The PHOBOS Glauber Monte Carlo*, 5, (2008)
[113] A. Majumder, Phys. Rev. D **85**, 014023 (2012)
[114] X. f. Guo and X. N. Wang, Phys. Rev. Lett. **85**, 3591 (2000)
[115] B. W. Zhang and X. N. Wang, Nucl. Phys. A **720**, 429 (2003)
[116] S. s. Cao, T. Luo, G. Y. Qin *et al*., Phys. Lett. B **777**, 255 (2018)
[117] R. B. Neufeld, Phys. Rev. D **83**, 065012 (2011)
[118] C. Shen, Z. Qiu, H. C. Song *et al*., Comput. Phys. Commun. **199**, 61 (2016)
[119] J. H. Putschke *et al*., *The JETSCAPE framework*, 3, (2019)
[120] F. Cooper and G. Frye, Phys. Rev. D **10**, 186 (1974)